A versatile waveguide source of photon pairs for chip-scale quantum information processing

Jun Chen,[1,2*] **Aaron J. Pearlman,**[1] **Alexander Ling,**[1,2] **Jingyun Fan,**[1,2†] **and Alan Migdall** [1,2]

[1] *Optical Technology Division, National Institute of Standards and Technology 100 Bureau Drive, Gaithersburg, MD 20899-8441, USA*

[2] *Joint Quantum Institute, University of Maryland, College Park, MD 20742, USA*

jun.chen@nist.gov, jfan@nist.gov

Abstract: We demonstrate a bright, bandwidth-tunable, quasi-phase-matched single-waveguide source generating photon pairs near 900 nm and 1300 nm. Two-photon coincidence spectra are measured at a range of operating temperatures of a periodically-poled $KTiOPO_4$ (PPKTP) waveguide, which supports both type-0 and type-II spontaneous parametric down-conversion. We map out relative contributions of two-photon to one-photon fluorescence for a range of operating parameters. Such a versatile device is highly promising for future chip-scale quantum information processing.

OCIS codes: (190.4410) Nonlinear Optics, parametric processes; (270.5585) Quantum information and processing; (230.7370) Waveguides.

References and links

1. P. G. Kwiat, K. Mattle, H. Weinfurter, A. Zeilinger, A. V. Sergienko, and Y. Shih, "New High-Intensity Source of Polarization-Entangled Photon Pairs," Phys. Rev. Lett. **75**, 4337-4341 (1995).
2. T. E. Kiess, Y. H. Shih, A. V. Sergienko, and C. O. Alley, "Einstein-Podolsky-Rosen-Bohm Experiment Using Pairs of Light Quanta Produced by Type-II Parametric Down-conversion," Phys. Rev. Lett. **71**, 3893-3897 (1993).
3. H. Takesue and K. Inoue, "Generation of polarization-entangled photon pairs and violation of Bell's inequality using spontaneous four-wave mixing in a fiber loop," Phys. Rev. A **70**, 031802(R) (2004).
4. X. Li, P. L. Voss, J. E. Sharping, and P. Kumar, "Optical-Fiber Source of Polarization-Entangled Photons in the 1550 nm Telecom Band," Phys. Rev. Lett. **94**, 053601 (2005).
5. A. L. Migdall, D. Branning, and S. Castelletto, "Tailoring single-photon and multiphoton probabilities of a single-photon on-demand source," Phys. Rev. A. **66**, 053805 (2002).
6. A. B. U'Ren, C. Silberhorn, K. Banaszek, and I. A. Walmsley, "Efficient Conditional Preparation of High-Fidelity Single Photon States for Fiber-Optic Quantum Networks," Phys. Rev. Lett. **93**, 093601 (2004).
7. E. Knill, R. LaFlamme, and G. J. Milburn, "A scheme for effcient quantum computation with linear optics," Nature **409**, 46-52 (2001).
8. P. Kok, W. J. Munro, K. Nemoto, T. C. Ralph, and G. J. Milburn, "Linear optical quantum computing with photonic qubits," Rev. Mod. Phys. **79**, 135-174 (2007).
9. K. Banaszek, A. B. U'Ren, and I. A. Walmsley, "Generation of correlated photons in controlled spatial modes by downconversion in nonlinear waveguides," Opt. Lett. **26**, 1367-1369 (2001).
10. S. Tanzilli, H. De Riedmatten, W. Tittel, H. Zbinden, P. Baldi, M. De Micheli, D.B. Ostrowsky, and N. Gisin, "Highly efficient photon-pair source using periodically poled lithium niobate waveguide," Electron. Lett. **37**, 26-28 (2001).
11. K. Sanaka, K. Kawahara, and T. Kuga, "New High-Efficiency Source of Photon Pairs for Engineering Quantum Entanglement," Phys. Rev. Lett. **86**, 5620-5623 (2001).
12. M. Fiorentino, S. M. Spillane, R. G. Beausoleil, T. D. Roberts, P. Battle, and M. W. Munro, "Spontaneous parametric down-conversion in periodically poled KTP waveguides and bulk crystals," Opt. Express **15**, 7479-7488 (2007).

13. Q. Zhang, X. Xie, H. Takesue, S. W. Nam, C. Langrock, M. M. Fejer, and Y. Yamamoto, "Correlated photon-pair generation in reverse-proton-exchange PPLN waveguides with integrated mode demultiplexer at 10 GHz clock," Opt. Express **15**, 10288-10293 (2007).
14. C. Liang, K. F. Lee, J. Chen, and P. Kumar, "Distribution of Fiber-Generated Polarization Entangled Photon-Pairs over 100 km of Standard Fiber in OC-192 WDM Environment," postdeadline paper presented at OFC 2006, paper PDP35.
15. S. Sauge, M. Swillo, S. Albert-Seifried, G. B. Xavier, J. Waldebäck, M. Tengner, D. Ljunggren, and A. Karlsson, "Narrowband polarization-entangled photon pairs distributed over a WDM link for qubit networks," Opt. Express **15**, 6926-6933 (2007).
16. W. P. Grice and I. A. Walmsley, "Spectral information and distinguishability in type-II down-conversion with a broadband pump," Phys. Rev. A **56**, 1627-1634 (1997).
17. Y. Kim and W. P. Grice, "Measurement of the spectral properties of the two-photon state generated via type II spontaneous parametric downconversion," Opt. Lett. **30**, 908-910 (2005).
18. H. S. Poh, C. Y. Lum, I. Marcikic, A. Lamas-Linares, and C. Kurtsiefer, "Joint spectrum mapping of polarization entanglement in spontaneous parametric down-conversion," Phys. Rev. A **75**, 043816 (2007).
19. A. Ling, P. Y. Han, A. Lamas-Linares, and C. Kurtsiefer, "Preparation of Bell States with controlled white noise," Laser Phys. **16**, 1140-1144 (2006).
20. M. M. Fejer, G. A. Magel, D. H. Jundt, and R. L. Byer, "Quasi-phase-matched second harmonic generation: tuning and tolerances," IEEE J. Quantum Electron. **28**, 2631-2654 (1992).
21. J. D. Bierlein and H. Vanherzeele, "Potassium titanyl phosphate: properties and new applications," J. Opt. Soc. Am. B **6**, 622-633 (1989).
22. M. Ghioni, A. Gulinatti, I. Rech, F. Zappa, and S. Cova, "Progress in silicon single-photon avalanche diodes," IEEE J. Sel. Top. Quantum Electron. **13**, 852-862 (2007).
23. K. M. Rosfjord, J. K. W. Yang, E. A. Dauler, A. J. Kerman, V. Anant, B. M. Voronov, G. N. Gol'tsman, and K. K. Berggren, "Nanowire single-photon detector with an integrated optical cavity and anti-reflection coating," Opt. Express **14**, 527-534 (2006).
24. A. E. Lita, A. J. Miller, and S. W. Nam, "Counting near-infrared single-photons with 95% efficiency," Opt. Express **16**, 3032-3040 (2008).
25. J. Chen, K. F. Lee, C. Liang, and P. Kumar, "Fiber-based telecom-band degenerate-frequency source of entangled photon pairs," Opt. Lett. **31**, 2798-2800 (2006).
26. J. Fan, A. Dogariu, and L. J. Wang, "Generation of correlated photon pairs in a microstructure fiber," Opt. Lett. **30**, 1530-1532 (2005).
27. K. F. Lee, J. Chen, C. Liang, X. Li, P. L. Voss, and P. Kumar, "Generation of high-purity telecom-band entangled photon pairs in dispersion-shifted fiber," Opt. Lett. **31**, 1905-1907 (2006).
28. H. Takesue and K. Inoue, "1.5-μm band quantum-correlated photon pair generation in dispersion-shifted fiber: suppression of noise photons by cooling fiber," Opt. Express **13**, 7832-7839 (2005).
29. S. D. Dyer, M. J. Stevens, B. Baek, and S. W. Nam, "High-efficiency, ultra low-noise all-fiber photon-pair source," Opt. Express **16**, 9966-9977 (2008).
30. J. Chen, "Development and Applications of Fiber-based Entanglement Sources", Ph.D. thesis, Northwestern University (2007), `http://terpconnect.umd.edu/~junchen/files/dissertation.pdf`.
31. J. Chen, X. Li, and P. Kumar, "Two-photon-state generation via four-wave mixing in optical fibers," Phys. Rev. A **72**, 033801 (2005).
32. D. C. Burnham and D. L. Weinberg, "Observation of Simultaneity in Parametric Production of Optical Photon Pairs," Phys. Rev. Lett. **25**, 84-87 (1970).
33. We note that another method for measuring joint spectrum is given by W. Wasilewski *et. al.*, "Joint spectrum of photon pairs measured by coincidence Fourier spectroscopy," Opt. Lett. **31**, 1130-1132 (2006).
34. C. K. Law, I. A. Walmsley, and J. H. Eberly, "Continuous frequency entanglement: effective finite Hilbert space and entropy control," Phys. Rev. Lett. **84**, 5304-5307 (2000).
35. A. B. U'Ren, C. Silberhorn, K. Banaszek, I. A. Walmsley, R. Erdmann, W. P. Grice, and M. G. Raymer, "Generation of pure-state single-photon wavepackets by conditional preparation based on spontaneous parametric downconversion," Laser Phys. **15**, 146-161 (2005).
36. A. Ekert and P. L. Knight, "Entangled quantum systems and the Schmidt decomposition," Am. J. Phys. **63**, 415-423 (1995).
37. A. B. U'Ren, K. Banaszek, and I. A. Walmsley, "Photon engineering for quantum information processing," Quant. Inf. and Comp. **3**, 480-502 (2003).
38. X. Li, P. L. Voss, J. Chen, K. F. Lee, and P. Kumar, "Measurement of co- and cross-polarized Raman spectra in silica fiber for small detunings," Opt. Express **13**, 2236-2244 (2005).
39. J. Fan and A. Migdall, "A broadband high spectral brightness fiber-based two-photon source," Opt. Express **15**, 2915-2920 (2007).
40. D. N. Klyshko, "Use of two-photon light for absolute calibration of photoelectric detectors," Sov. J. Quantum Electron. **10**, 1112-1117 (1980).
41. A. Fedrizzi, T. Herbst, A. Poppe, T. Jennewein, and A. Zeilinger, "A wavelength-tunable fiber-coupled source of

narrowband entangled photons," Opt. Express **15**, 15377-15386 (2007).
42. S. Sauge, M. Swillo, M. Tengner, and A. Karlsson, "A single-crystal source of path-polarization entangled photons at non-degenerate wavelengths," Opt. Express **16**, 9701-9707 (2008).
43. T. Y. Fan, C. E. Huang, B. Q. Hu, R. C. Eckardt, Y. X. Fan, R. L. Byer, and R. S. Feigelson, "Second harmonic generation and accurate index of refraction measurements in flux-grown $KTiOPO_4$," App. Opt. **26**, 2390-2394 (1987).
44. B. Boulanger, I. Rousseau, J. P. Feve, M. Maglione, B. Menaert, G. Marnier, "Optical Studies of Laser-Induced Gray-Tracking in KTP," IEEE J. Quantum Electron. **35**, 281-286 (1999).

1. Introduction

Photon pairs have been an essential ingredient in many modern quantum-optical applications such as entanglement generation [1, 2, 3, 4], heralded single-photon sources [5, 6], and linear optical quantum computing [7, 8]. In recent years, spontaneous parametric down-conversion (SPDC) in periodically-poled nonlinear waveguides has been shown to be an efficient way to generate such correlated photons [9, 10, 11, 12, 13]. SPDC is a second-order [$\chi^{(2)}$] nonlinear process wherein a pump photon is absorbed and a pair of energy- and momentum-conserving daughter photons (referred to as signal and idler) are generated, satisfying $\omega_{\rm p} = \omega_{\rm s} + \omega_{\rm i}$ and $\vec{k}_{\rm p} = \vec{k}_{\rm s} + \vec{k}_{\rm i}$, where $\omega_{\rm p,s,i}$ and $\vec{k}_{\rm p,s,i}$ are the photon frequencies and wave-vectors, and the subscripts p, s, and i stand for pump, signal, and idler, respectively. Compared with its bulk-crystal counterpart which generates photon pairs in an inherently multi-spatial-mode cone-like pattern [1], SPDC in waveguides outputs photon pairs collinearly, with the predominant component in a single transverse spatial mode [9, 12]. This makes it easier to efficiently collect these photons using single-mode optical fibers, and offers the potential to make chip-scale devices for quantum-information-processing applications.

To fully utilize the potential of such a chip-scale quantum device, it is necessary to understand its various operating modes, such as the temperature and pump-polarization dependencies of the photon-pair production rate. More importantly, for wavelength-division-multiplexing applications that use many wavelength pairs simultaneously [14, 15], one needs to have precise knowledge of the coincidence spectra (also known as joint spectra) [16, 17, 18, 19], and be able to separate true signal (photon pairs) from random noise (single-photon fluorescence [6, 12]). This critical information is missing from current literature. In this paper, we present a first step in systematically studying a waveguide-based photon-pair source. Both photon-pair and single-photon emission spectra, as well as their dependence on input-pump polarization and waveguide temperature, are obtained for both type-0 and type-II phase-matching SPDC processes in a single PPKTP waveguide.

2. Experimental setup

Figure 1 depicts our experimental setup. The pump beam, derived from an 80-MHz pulsed laser with $\lambda_{\rm p} = 532.2\,$nm and a 5-ps pulse width, is sent through a spatial filter and a prism to ensure that the PPKTP waveguide is pumped with a single spatial-mode and spectrally clean beam (i.e., the pump beam does not contain any frequency components at either the signal or the idler frequencies). The waveguide is 1.5-cm long with a $4 \times 4\,\mu{\rm m}^2$ cross section. It was fabricated on a flux-grown type-II ($H_{\rm p} \rightarrow V_{\rm s} + H_{\rm i}$, H: horizontal polarization, V: vertical polarization) KTP crystal, and then periodically poled with a nominal grating period of $\Lambda = 8.29\,\mu$m to support type-0 ($V_{\rm p} \rightarrow V_{\rm s} + V_{\rm i}$) quasi-phase matching (QPM). QPM is enabled by periodically poling the nonlinear crystal so that the interaction length of the pump inside the crystal can be extended and a desired phase-matched set of wavelengths can be engineered, satisfying $k_{\rm p} = k_{\rm s} + k_{\rm i} + 2\pi m/\Lambda + k_{\rm wg}$ [20, 12], where m, an integer, is the mth order harmonic of the grating, and $k_{\rm wg}$ is the waveguide contribution to phase matching [12]. As a result, the

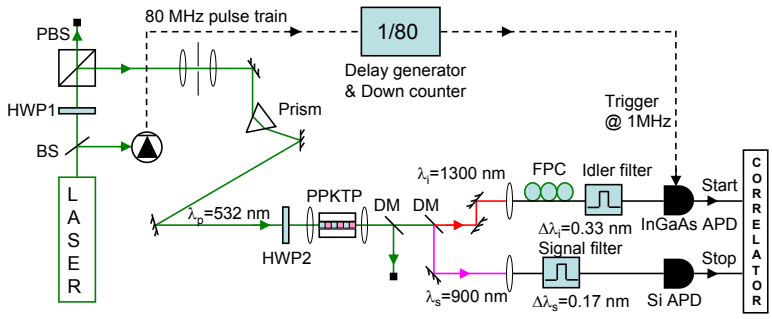

Fig. 1: Diagram of the experimental setup. A PPKTP waveguide is pumped with a pulsed laser, and the down-converted photons are spectrally analyzed using tunable filters and coincidence detection with single-photon detectors. BS, beam splitter; PBS, polarizing beam splitter; DM, dichroic mirror; HWP, half-wave plate; FPC, fiber polarization controller; APD, avalanche photodiode.

waveguide can support both type-0 and type-II SPDC processes, with its emission field predominantly in a single spatial mode. Note that type-0 SPDC is only possible with the technique of QPM, whereas type-II SPDC is enabled by the KTP crystal itself. The detailed mechanisms of the phase matching for these two types of SPDC will be analyzed in section 3.5. Measured values [21] of nonlinear susceptibility tensor components, or its contracted-notation counterparts (commonly known as nonlinear-optical coefficients) show that at the wavelength of 1.064 μm, $d_{33} = 13.7$ pm/V (responsible for type-0 SPDC) and $d_{24} = 7.6$ pm/V (responsible for type-II SPDC). The QPM-induced effective nonlinear-optical coefficient for type-0 SPDC is $d_{\text{eff}} = \frac{2}{\pi} d_{33} \approx 8.7\,\text{pm/V} > d_{24}$. This suggests that type-0 SPDC could be made potentially more effective than type-II SPDC, but as will be shown in our experimental results, the reverse is true for this particular waveguide at its phase-matched wavelengths. We note that while this PPKTP waveguide was designed to support type-0 SPDC, it also happens to still phase-match type-II SPDC. The existence of two types of SPDC is neither necessary nor directly related to our goal of providing precise characterization of waveguide-based coincidence spectra, but can be seen as the waveguide's versatile ability to produce different kinds of two-photon states just by tuning the pump polarization.

At the waveguide input, a half-wave plate (HWP2 in Fig. 1) is used to control the pump polarization to switch between the two types of SPDC. The waveguide's temperature is controlled using a thermo-electric cooler with 0.01 °C stability. We use an aspheric lens [numerical aperture (NA) = 0.2] to couple pump light into the waveguide (NA $\approx$ 0.2), and a 10X microscope to couple out light of all wavelengths. The coupling efficiency of the pump into the waveguide is about 30 %. The daughter photons are separated from the pump beam and from each other by using two dichroic mirrors. Since the signal ($\lambda_s \approx 900$ nm) and idler ($\lambda_i \approx 1300$ nm) photons are quite different in wavelength, their spatial modes evolve differently when they emerge from the waveguide. We optimize the coupling of idler photons into a single-mode fiber by adjusting the output 10X microscope to nearly collimate its output. With the idler mode now optimized, the spatial mode of the signal photons is observed (using a CCD camera) to be slightly converging, which we correct using a concave lens ($f = -200$ mm, not shown in Fig. 1) before coupling into a separate single-mode fiber. The non-degeneracy of the signal and idler wavelengths made their separation from each other and the bright pump light easy to accomplish; we find that in practice two dichroic mirrors (DM in Fig. 1) are enough to provide the necessary

pump rejection ($> 100\,$dB) to effectively detect the signal and idler photons. This particular set of wavelengths would be useful, for example, in a hybrid quantum communication system, wherein the idler photon ($\approx 1300\,$nm, a telecom wavelength) of a correlated pair propagates through a low-loss telecom fiber, and its sibling — the signal photon ($\approx 900\,$nm) — can be sent through free space with relatively low loss. Finally, both photons can be detected using high quantum efficiency single-photon detectors available with current technology [22, 23, 24].

The filter system for the signal photons is a homemade double-grating filter with both a tunable central wavelength and an adjustable bandwidth, while for the idler photons we use a commercial fixed-bandwidth tunable filter. Both filters are computer controlled for automatic spectral scanning. The signal filter bandwidth is set to $\Delta\lambda_s = 0.17\,$nm to match the fixed bandwidth of the idler filter ($\Delta\lambda_i = 0.33\,$nm), so that they contain the same frequency bandwidths. After filtering, idler photons are detected with an InGaAs avalanche photodiode in gated Geiger mode, with a 1 MHz gate frequency and a gate width of 1.28 ns. The gating signal is obtained by using a beam splitter (BS in Fig. 1) to pick off a part of the laser output, which is detected with an analogue photodiode. The 80 MHz detection output is then sent through a down-counter/delay generator and converted to a 1 MHz pulse train with suitable delay. A fiber polarization controller (FPC in Fig. 1) is placed in front of the idler filter to maximize its transmission which is polarization dependent. Signal photons are detected with a silicon avalanche single-photon detector. Coincidences are recorded through start and stop inputs, with the detection pulses from the idler (signal) acting as the start (stop).

3. Experimental results

3.1. Temperature dependence of single-photon spectra

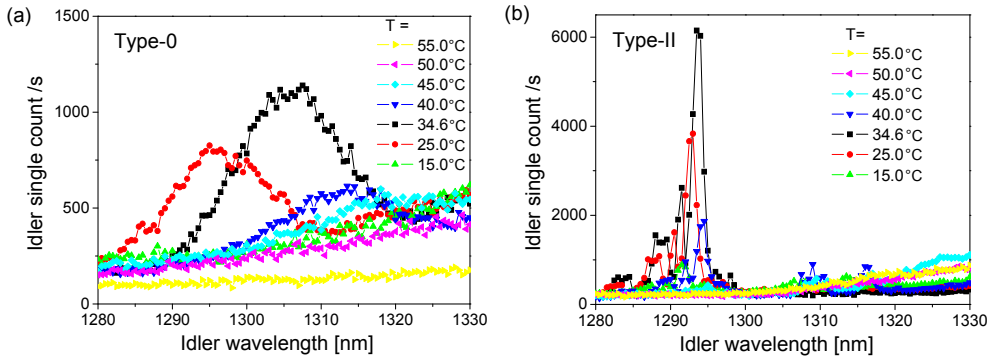

Fig. 2: Temperature dependence of idler single-count spectrum for (a) type-0 SPDC, and (b) type-II SPDC.

The temperature dependencies of single-count idler spectra for both types of SPDC are shown in Fig. 2. We scan the computer-controlled idler-channel tunable filter for each waveguide temperature value (at a step size of 0.5 nm) and record the idler single counts. The average pump power exiting the waveguide is kept at 0.5 mW for both *H* and *V* pump polarizations. Note that these counts are taken without any measurement on the signal channel (i.e., they are not heralded counts). For both types of SPDC, we observe a dramatic dependence of single-photon production rate on temperature. While we cannot ascertain that all of the collected photons are produced by SPDC (in fact, a portion of them are produced by single-photon fluorescence due to defects in the waveguide [6, 12]), we conjecture that the peaks in the single-photon spectra are much more likely to be caused by the SPDC photons rather than fluorescence, and they

also correspond to peaks in the production of SPDC photon pairs. This conjecture is confirmed by measurements of the coincidence spectra in section 3.3. On the other hand, at temperatures that do not allow efficient quasi-phase matching (e.g., $T = 55.0\,^{\circ}\mathrm{C}$), almost all of the collected photons are produced by single-photon fluorescence, since no peak structure in the single-count spectrum is observable.

Comparing Fig. 2(a) and (b), we can see that: (i) both types of SPDC have an optimal operating temperature, which is nearly the same ($T_{\mathrm{opt}} = 34.6\,^{\circ}\mathrm{C}$); (ii) type-0 SPDC has a much wider phase-matching bandwidth [full width at half maximum (FWHM) $\approx 12\,\mathrm{nm}$ for idler] than type-II SPDC (FWHM $\approx 1.4\,\mathrm{nm}$ for idler); (iii) type-II SPDC is spectrally brighter (5X) than type-0 SPDC at their peak values, and (iv) in terms of the overall brightness (i.e., unfiltered output), we find that type-II is slightly brighter ($\sim 7\%$) than type-0 at the optimal temperature T_{opt}. The same characteristics are also seen in the signal single-count spectra (not shown). We must acknowledge the unexpected coincidence that both type-0 and type-II SPDC are phase matched at the same optimal temperature. While it is possible that this is simply a coincidence, it is more likely that there is some physical reason, although at this point we have not found it. As to the differences in terms of bandwidths and brightnesses between Fig. 2(a) and (b), a combination of two factors is responsible. First, because the PPKTP waveguide is birefringent, a horizontally-polarized pump travels at a different group velocity than a vertically-polarized pump, and therefore must satisfy a different phase-matching condition for efficient down-conversion, which gives rise to the different phase matching bandwidths for the two types of SPDC. Second, the two types of SPDC processes rely on different second-order nonlinear susceptibility tensor components: $\chi^{(2)}_{zzz}$ (or $d_{\mathrm{eff}} = \frac{2}{\pi} d_{33}$) for type-0 and $\chi^{(2)}_{zyy}$ (or d_{24}) for type-II. One might think that this helps to explain why type-II is brighter both spectrally and in overall output than type-0. However, comparing the magnitudes of the nonlinear-optic coefficients alone would lead one to draw the opposite conclusion, since $d_{\mathrm{eff}} > d_{24}$. To solve this dilemma and to offer deeper insight into the phase matching mechanisms for the two types of SPDC in a waveguide, we will compare the two processes in more detail in section 3.5, and provide a possible reason for why this is the case.

3.2. Coincidence-to-accidental ratio

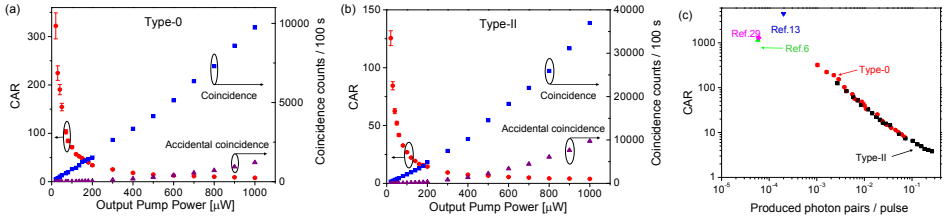

Fig. 3: Pump power dependencies of CAR (left axis) and coincidences and accidental coincidences per 100 s (right axis) for (a) type-0 SPDC with $\lambda_{\mathrm{s}} = 899.18\,\mathrm{nm}$ and $\lambda_{\mathrm{i}} = 1304.00\,\mathrm{nm}$ and (b) type-II SPDC with $\lambda_{\mathrm{s}} = 904.00\,\mathrm{nm}$ and $\lambda_{\mathrm{i}} = 1294.00\,\mathrm{nm}$. (c) Log-log plot of CAR vs. produced photon pairs per pulse. Three additional data points from external references are included for comparison. Detector dark-count contributions have been subtracted.

To collect the peak phase-matched SPDC photon pairs at the optimal temperature T_{opt}, we set the tunable filters in both channels. For type-0, we use the wavelength pair $\{\lambda_{\mathrm{s}} = 899.18\,\mathrm{nm}, \lambda_{\mathrm{i}} = 1304.00\,\mathrm{nm}\}$; for type-II: $\{\lambda_{\mathrm{s}} = 904.00\,\mathrm{nm}, \lambda_{\mathrm{i}} = 1294.00\,\mathrm{nm}\}$. For each wavelength pair, we varied the pump power (by rotating HWP1 in Fig. 1) and recorded coincidences and accidental coincidences at each pump power level. The coincidence-to-accidental ratio (CAR), a

commonly used two-photon source purity measure [25, 26, 27, 28], is plotted as a function of the output pump power in Fig. 3. The CAR values for our source for both types of SPDC are comparable with other sources at similar pair production rates [6, 13, 29].

The CAR also shows a trend common to the other photon sources: it monotonically decreases with increasing pump power. This is understood because the coincidence counts per pulse C is roughly proportional to the pump power P (i.e., $C \propto P$), whereas accidental coincidence counts per pulse A scales as P^2 (i.e., $A \propto P^2$), so CAR $\equiv C/A \propto 1/P$. The peak structure observed in other photon sources (i.e., the CAR reaches a maximum at an "optimum" low pump power, below which the CAR starts to decrease) is missing here, which is possibly due to the low dark-count rates of about 4.4×10^{-5}/gate for the InGaAs detector and 3.8×10^{-6}/gate for the silicon detector (subtracted from the data shown in Fig. 3). Even at the lowest average pump power used in the experiment, $P = 20\,\mu$W for type-0 SPDC, our detected mean photon number is $\approx 6.3 \times 10^{-5}$/gate for the signal channel and $\approx 6.6 \times 10^{-5}$/gate for the idler channel, which are still larger than both detectors' dark-count rates. We believe this is the main reason why we do not observe the characteristic peak structure in CAR, which usually occurs in the region where detector dark counts dominate. Therefore, we expect the CAR peak to appear once we reach a sufficiently low pump power level. This, however, will in general lead to a prohibitively long integration time due to low count rates. For a detailed theoretical modelling of CAR, see section 5.3 of Ref. [30], whose derivation uses a generic Bogoliubov transformation that is equally valid for four-wave mixing and SPDC. We note in passing that if the filter bandwidths are broadened relative to the pump bandwidth, the CAR value will decrease as more uncorrelated photons are collected in the process [31].

We also see that type-II SPDC has a lower CAR than type-0 SPDC at the same pump power; however, this is because type-II SPDC produces more coincidences than type-0 SPDC at the same pump power. In other words, type-II SPDC is more efficient than its type-0 counterpart in this waveguide, so it requires a lower pump power for achieving the same CAR. Indeed, if we plot CAR against pair production efficiency (i.e., produced photon pairs per pulse) as shown in Fig. 3(c), we can see that the two SPDC processes have about the same CAR at the same level of pair production efficiency. A high CAR, which suggests a high-purity photon-pair source, can be achieved for both types of SPDC when the waveguide is pumped with relatively low peak pump power, which incurs low pair production per pulse. Of course, the photon pair production rate (i.e., pairs/s) can still be made quite high if one uses a high-repetition-rate pump laser (see for instance Ref. [13]).

To compare our source with other photon pair sources, we include three additional data points in Fig. 3(c) from Ref. [6] (type-II SPDC in a PPKTP waveguide), Ref. [13] (quasi-phase matched SPDC in a PPLN waveguide), and Ref. [29] (four-wave mixing in a liquid-helium-cooled dispersion-shifted fiber). Fig. 3(c) clearly shows the tradeoff between CAR and the pairs per pulse production rate. By extrapolating our CAR-vs.-production-rate data, we can see that the sources in Refs. [6] and [29] are not as good as our waveguide while the source in Ref. [13] may be superior to our source. This could be due to a number of reasons, including less emission of noise photons, lower propagation loss, and higher photon-pair production efficiency in the PPLN waveguide.

3.3. Coincidence spectra

The spectra presented in section 3.1 are useful for identifying the optimum operating temperatures for the waveguide. However, as we have pointed out, single-photon spectra do not distinguish between photons that come from single-photon fluorescence and those generated in a SPDC process. A standard technique to discriminate against single-photon fluorescence is to measure coincidences during the spectral scan [32]. The single-photon fluorescence will not

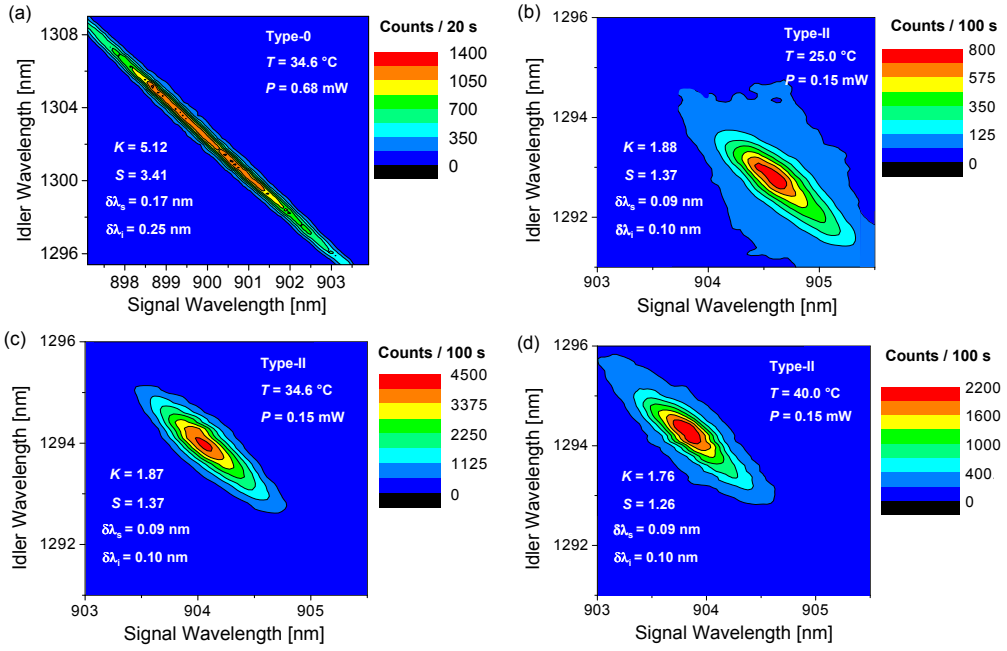

Fig. 4: Coincidence spectra for (a) type-0 SPDC at $T_{\text{opt}} = 34.6\,^{\circ}\text{C}$, type-II SPDC at (b) $T = 25.0\,^{\circ}\text{C}$, (c) $T_{\text{opt}} = 34.6\,^{\circ}\text{C}$, and (d) $T = 40.0\,^{\circ}\text{C}$. Note that while the range and scale of (a) are different from (b), (c), and (d), the aspect ratio is constant at 2:1 for all; and although the power P and counting time t of (a) are different from (b), (c), and (d), their product Pt is roughly the same for all, so that the results can be directly compared. The Schmidt number K and entropy of entanglement S are also indicated on each figure.

show up on a coincidence measurement except by accident (such events are known as accidental coincidences, and can be generated by, for instance, a coincidence between a detector dark count and a registered single-photon fluorescence).

Furthermore, recording the coincidence spectra is important for experiments in entanglement. It is known that Type-II SPDC which is pumped by a pulsed (and hence broadband) laser results in spectrally distinguishing properties for the down-converted photons [16]. When correlated photon pairs from such a pulsed source are used to generate polarization-entangled photon pairs, these spectral properties can cause the entanglement quality to suffer considerably. Such spectral properties show up readily in a coincidence-based spectral scan, which we call the coincidence spectrum (or joint spectrum, as they reveal the joint spectral properties of the correlated photon pair). Although several groups have studied the coincidence spectra of pulsed Type-II sources pumped by ultrafast lasers (pulse duration ≈ 10 — 200 fs) [17, 18], no such spectra exist for sources based on waveguides that are pumped with slower pulses (≈ 2 — 10 ps), the regime where we operate. To understand whether the spectral features present in ultrafast sources also exist in our system, we have mapped out the coincidence spectra for both type-0 and type-II SPDC processes.

To measure a coincidence spectrum of each type of SPDC, we use two narrow-band computer-controlled tunable filters, one in each collection arm [33]. Stepping through the signal and idler wavelength ranges, we record coincidence counts for each $\{\lambda_{\text{s}}, \lambda_{\text{i}}\}$ pair with $\{\Delta\lambda_{\text{s}}, \Delta\lambda_{\text{i}}\}$ resolution at a discrete step size of $\{\delta\lambda_{\text{s}}, \delta\lambda_{\text{i}}\}$. The results are color-coded as 2-

dimensional coincidence spectra shown in Fig. 4. The wavelength resolutions are kept the same for all measurements ($\Delta\lambda_s = 0.17\,\text{nm}$, $\Delta\lambda_i = 0.33\,\text{nm}$), and the step sizes used in obtaining each coincidence spectrum are indicated on the figures. Note that the resolutions in this experiment are limited not by our homemade signal grating filter, but by the fixed passband of the commercial idler filter.

We also include two important quantities on each coincidence spectrum, namely, the Schmidt number K (also known as the cooperativity parameter) and the entropy of entanglement S [34, 35]. They quantify how much spectral entanglement (or nonseparability) exists in a given two-photon state $\Psi(\lambda_s, \lambda_i)$, and can be conveniently calculated from its coincidence spectrum through Schmidt decomposition [36]. In terms of the normalized Schmidt engenvalues λ_n (i.e., $\sum_n \lambda_n = 1$), the Schmidt number is defined as $K = 1/(\sum_n \lambda_n^2)$ and the entropy of entanglement is given by $S = -\sum_n \lambda_n \log_2(\lambda_n)$. Both of these increase monotonically with the amount of spectral entanglement present in $\Psi(\lambda_s, \lambda_i)$. They achieve their minimum values ($K_{\text{min}} = 1$ and $S_{\text{min}} = 0$) for a factorable two-photon state [i.e., $\Psi(\lambda_s, \lambda_i) = \psi(\lambda_s)\phi(\lambda_i)$, possessing zero spectral entanglement], which is an important resource for quantum information applications such as heralded pure single-photon states [35] and multi-element Hong-Ou-Mandel interference [37]. The Schmidt number is estimated to be 5.12 for the type-0 two-photon state shown in Fig. 4(a), indicating a high degree of spectral entanglement. In comparison, the Schmidt numbers are much lower ($K \approx 1.8$) for the type-II two-photon states shown in Fig. 4(b), (c) and (d). This means that the type-II two-photon state is less spectrally entangled than its type-0 counterpart in this waveguide, and thus more closely approaches a factorable state. This also suggests that a factorable two-photon state output is possible through waveguided SPDC.

Comparing Fig. 4(a) and (c), we can see that type-0 SPDC has a wider phase-matching bandwidth, but is spectrally dimmer than type-II SPDC, which is consistent with the single-count data shown in Fig. 2. Comparisons among Fig. 4(b), (c), and (d) reveal that the coincidence spectrum maintains its characteristic shape at different temperatures, albeit with some changes in the peak count rate and the peak wavelengths. They also show the same optimal temperature for type-II single-photon [Fig. 2(b)] and pair production. We have also taken coincidence spectra for type-0 SPDC at different temperatures (not shown), which point to the same conclusion. This proves our initial conjecture posed in section 3.1, namely, the two optimal temperatures coincide. It is noteworthy that the shape of the coincidence spectra is very similar to the spectra of CW-based sources [17, 19], and unlike the irregular shaped spectra reported with ultrafast sources [18]. The similarity between our source and the CW sources can be understood since our pump bandwidth is relatively narrow ($\approx 0.2\,\text{nm}$) and can be effectively treated as quasi-CW. The difference between our source and ultrafast sources is mainly caused by a combination of different phase-matching curves for the materials used and the pump bandwidths involved. Nevertheless, this means that spectral distinguishability is not an issue when considering if a waveguide pumped with picosecond lasers can be used as a source for polarization-entangled photon pairs. Although both types of SPDC contain some degree of spectral entanglement (as evidence by the non-vanishing S in both cases), tight spectral filtering can be applied to reduce the amount of spectral entanglement to allow efficient quantum information processing applications such as polarization entanglement swapping, at the cost of reduced coincidence count rates.

3.4. Photon pair and single-photon fluorescence

From these coincidence-spectrum measurements, one can extract the photon-pair component from the single-photon fluorescence component in each channel. We denote η_s (η_i) as the total efficiency (including all collection and detection losses) for the signal (idler) photon channels. The photon-pair contribution to the total photon flux produced by the waveguide can be written

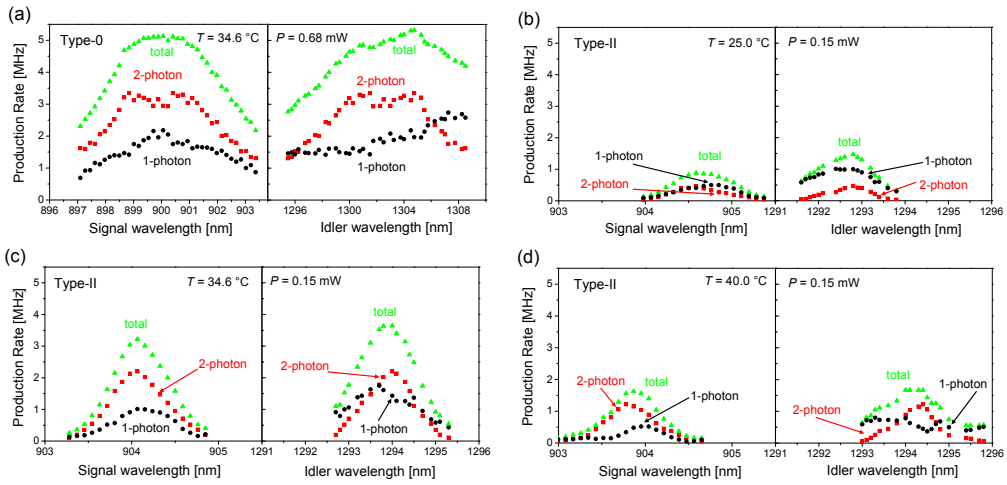

Fig. 5: Single-count spectra for (a) type-0 SPDC at $T_{\mathrm{opt}} = 34.6\,^{\circ}\mathrm{C}$, type-II SPDC at (b) $T = 25.0\,^{\circ}\mathrm{C}$, (c) $T_{\mathrm{opt}} = 34.6\,^{\circ}\mathrm{C}$, and (d) $T = 40.0\,^{\circ}\mathrm{C}$. Note that the production rate is plotted instead of the detected rate. Photon-pair (2-photon) and single-photon background (1-photon) contributions are distinguished using experimentally determined total collection efficiencies.

Table 1: Measured values of transmission efficiencies for optical path components and the single-photon detection efficiencies. The uncertainties are specified in one standard deviation.

Component	Channel efficiencies (%)	
	Signal	Idler
Waveguide out-coupling	91 ± 1	80 ± 1
Free-space optics	82 ± 1	76 ± 1
Fiber coupling	25 ± 2	45 ± 2
Filter transmission	50 ± 1	49 ± 1
Single-photon detection	38 ± 1	30 ± 1
Total	3.5 ± 0.3	4.0 ± 0.2

as: $N_2 = (N_{\mathrm{c}} \cdot F)/(\eta_{\mathrm{s}} \cdot \eta_{\mathrm{i}})$, where $N_{\mathrm{c}} \equiv C - A$ is the detected true coincidence rate and $F = 80$ is the down-count factor. The single-photon fluorescence production rate can be calculated by subtracting the photon-pair rate from the total production rate in each channel: $N_{1(\mathrm{s})} = D_{\mathrm{s}}/\eta_{\mathrm{s}} - N_2$ and $N_{1(\mathrm{i})} = D_{\mathrm{i}} \cdot F/\eta_{\mathrm{i}} - N_2$, where D_{s} and D_{i} are the dark-count-subtracted detected photon rate in the signal and idler channel, respectively. This technique is similar to the one used in separating four-wave-mixing photon pairs from spontaneous Raman scattering in the context of fiber-based $\chi^{(3)}$ photon-pair sources [38, 39]. In the following, we apply this to our waveguide-based $\chi^{(2)}$ photon-pair source, and for the first time give a complete and separate description of the SPDC photon spectrum and fluorescence spectrum for the entire down-conversion bandwidth, for both types of SPDC.

The results in Fig. 5 show the relative strength of down-converted photon pair and single-photon fluorescence for type-0 SPDC at its optimal temperature [Fig. 5(a)] and type-II SPDC at three different temperatures [Fig. 5(b), (c), (d)]. In the analysis, we used the experimentally determined total collection efficiencies $\eta_{\mathrm{s}} = 3.5\,\% \pm 0.3\,\%$ and $\eta_{\mathrm{i}} = 4.0\,\% \pm 0.2\,\%$. The details of the measured efficiencies are listed in Table 1. These efficiencies were measured for a pair

of wavelengths $\lambda_s = 900\,\text{nm}$ and $\lambda_i = 1300\,\text{nm}$ using classical light at those wavelengths. It is possible that these efficiencies are dependent on the wavelength of light that is collected. However, since the majority of the down-converted 1300 nm (900 nm) light is emitted in a single spatial mode, and falls within the 12 nm and 1.4 nm (6 nm and 0.7 nm) bands for type-0 and type-II SPDC, respectively, we assume the collection efficiencies are constant within those passbands. It can be clearly seen that when operating at the optimal temperature, the photon-pair component is much higher than the single-photon fluorescence component. On the other hand, the single-photon fluorescence can become comparable to or even higher than the former when the waveguide is away from the optimal temperature or the photon wavelength falls outside the SPDC phase-matching band.

These measured efficiencies can be compared with the so-called Klyshko efficiencies [40], which are defined as $\eta^{\text{K}}_{\text{s(i)}} \equiv \frac{C}{D_{\text{i(s)}}}$, where C is the coincidence counts per pulse, and D_j (j=s,i) is the detected single counts per pulse in the jth channel. The Klyshko efficiencies are calculated to be $\eta^{\text{K}}_{\text{s}} = 2.3\% \pm 0.1\%$ and $\eta^{\text{K}}_{\text{i}} = 2.5\% \pm 0.1\%$ for both types of SPDC. They are less than their measured counterparts, i.e., $\eta^{\text{K}}_{\text{s(i)}} < \eta_{\text{s(i)}}$. This is because the photon source that we have is not a *pure* photon-pair source, i.e., one that outputs photon pairs and *only* photon pairs. For a pure photon-pair source, one would have $D_{\text{s}} = \eta_{\text{s}}\mu$, $D_{\text{i}} = \eta_{\text{i}}\mu$, and $C = \eta_{\text{s}}\eta_{\text{i}}\mu$, where μ is the produced photon pair per pulse. Therefore, from the definition of the Klyshko efficiencies, we have $\eta^{\text{K}}_{\text{s(i)}} \equiv \frac{C}{D_{\text{i(s)}}} = \eta_{\text{s(i)}}$. Our waveguide source, in contrast, has both photon pairs and single-photon fluorescence in its output. Such a source can be modelled by including a noise term $\mu_{\text{s(i)}}$ in the single photon production rate, i.e., $D'_{\text{s}} = \eta_{\text{s}}(\mu + \mu_{\text{s}})$, $D'_{\text{i}} = \eta_{\text{i}}(\mu + \mu_{\text{i}})$, and $C' = \eta_{\text{s}}\eta_{\text{i}}\mu$, where $\mu_{\text{s(i)}}$ is the produced single-photon noise per pulse. Note that here C' stands for *true* coincidence, where accidental coincidence counts from noise photons and multiple photon pairs should be subtracted ($C' = C - A$). As a result, we have for our waveguide source, $\eta^{\text{K}}_{\text{s(i)}} \equiv \frac{C'}{D'_{\text{i(s)}}} = \frac{\mu}{\mu+\mu_{\text{i(s)}}}\eta_{\text{s(i)}} < \eta_{\text{s(i)}}$, which is consistent with our measured and calculated results.

Table 2: Comparison of spectral brightness efficiencies for both type-0 and type-II SPDC for our waveguide versus the results of others (Refs. [12, 41, 42]). Note that while Ref. [42] specifies an *in-fiber* spectral brightness efficiency, all other numbers are *pair-production* spectral brightness efficiencies (i.e., without coupling into single-mode fibers).

References	SPDC spectral brightness efficiency (10^6/s/mW/THz)	
	type-0	type-II
Previous work	3 [42]	160 [12, 41]
This work	83	250

From Fig. 5 one can also estimate our source's spectral brightness per mW of pump power exiting the waveguide, which we define as "spectral brightness efficiency." The pair-production spectral brightness efficiency for the optimal temperature and the peak wavelength pair for type-0 SPDC is $\approx 8.3 \times 10^7$/s/mW/THz, and for type-II SPDC is $\approx 2.5 \times 10^8$/s/mW/THz. These numbers are the highest spectral brightness efficiencies reported to date (see Table 2 for a detailed comparison).

3.5. Quasi-phase matching for type-0 and type-II SPDC

To further our understanding of the physical mechanisms of QPM in the PPKTP waveguide, we numerically calculate the phase-matching curves for both types of SPDC using the Sellmeier equations for flux-grown bulk PPKTP given in Ref. [43]. As depicted in Fig. 6(a), x is the light propagation direction in the waveguide, y is the horizontal polarization, and z is the vertical

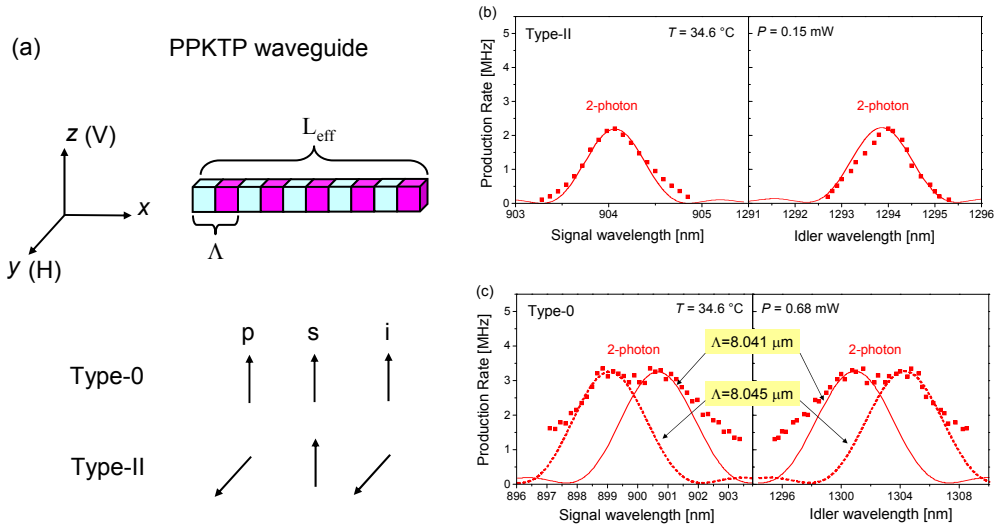

Fig. 6: (a) Schematic of the two types of phase matching schemes inside our PPKTP waveguide. Quasi-phase matching functions adjusted to match the photon-pair components obtained from experimental data for (b) type-II SPDC at $T_{\rm opt} = 34.6\,^{\circ}$C, and (c) type-0 SPDC at $T_{\rm opt} = 34.6\,^{\circ}$C. Solid squares are data points for photon-pair components derived from Fig. 5. Fit parameters are $L_{\rm eff} = 8.5\,$mm and $k_{\rm wg} = -0.1\,\mu{\rm m}^{-1}$ for all curves in (b) and (c). The dashed and the solid curve in (c) use the poling period values indicated.

polarization. The Sellmeier equations for *y*-polarized and *z*-polarized light fields in the PPKTP waveguide are [43]:

$$n_y(\lambda) = \sqrt{2.19229 + \frac{0.83547}{1 - 0.04970\,\lambda^{-2}} - 0.01621\,\lambda^2}\,, \tag{1}$$

$$n_z(\lambda) = \sqrt{2.25411 + \frac{1.06543}{1 - 0.05486\,\lambda^{-2}} - 0.02140\,\lambda^2}\,, \tag{2}$$

where $n_{y(z)}$ is the refractive index for *y* (*z*)-polarized light. The phase-matching equations for type-0 and type-II SPDC in the waveguide are given by:

$$\frac{2\pi\, n_z(\lambda_{\rm p})}{\lambda_{\rm p}} = \frac{2\pi\, n_z(\lambda_{\rm s})}{\lambda_{\rm s}} + \frac{2\pi\, n_z(\lambda_{\rm i})}{\lambda_{\rm i}} + \frac{2\pi\, m_0}{\Lambda} + k_{\rm wg}\,, \tag{3}$$

$$\frac{2\pi\, n_y(\lambda_{\rm p})}{\lambda_{\rm p}} = \frac{2\pi\, n_z(\lambda_{\rm s})}{\lambda_{\rm s}} + \frac{2\pi\, n_y(\lambda_{\rm i})}{\lambda_{\rm i}} + \frac{2\pi\, m_2}{\Lambda} + k_{\rm wg}\,, \tag{4}$$

where the wavelengths are in microns, and m_0 (m_2) is the (integer) order of grating harmonic that contributes to phase matching in type-0 (type-II) SPDC.

In the above equations, we assume the waveguide contribution $k_{\rm wg}$ to phase matching is the same for the two types of SPDC, which is a valid assumption since the wavelengths involved are very close. Solving Eqs. 3 and 4 simultaneously, we find valid solutions *only when* $m_0 = 1$ and $m_2 = 0$. This means that type-II phase matching does not need any contribution from periodic poling, and therefore picks up the 0th-order harmonic of the grating ($m_2 = 0$), whereas type-0 phase matching is made possible by the contribution from the first-order harmonic of the grating ($m_0 = 1$).

Putting the peak phase matching wavelengths for type-II SPDC ($\lambda_p = 0.5322\,\mu$m, $\lambda_s = 0.904\,\mu$m, and $\lambda_i = 1.294\,\mu$m) into Eq. 4 determines the waveguide contribution to be $k_{wg} = -0.1\,\mu\text{m}^{-1}$. Similarly, by plugging the peak phase matching wavelengths for type-0 SPDC ($\lambda_p = 0.5322\,\mu$m, $\lambda_s = 0.8992\,\mu$m, and $\lambda_i = 1.304\,\mu$m) into Eq. 3, we determine the fit value of the grating period to be $\Lambda \approx 8.045\,\mu$m. This is less than the nominal value of $8.29\,\mu$m given by the manufacturer, and we attribute this difference to the temperature dependence of the grating period and possible variations in the periodic poling process (since the poling period is only microns long, there may be variations in uniformity of pole widths and periods).

In the CW pump limit (a good approximation for our pump due to its narrow bandwidth), the signal and idler spectra are given by the function $\text{sinc}^2(\Delta k L_{\text{eff}}/2)$, where $\Delta k = k_p - k_s - k_i - k_{wg}$ for type-II SPDC and $\Delta k = k_p - k_s - k_i - 2\pi/\Lambda - k_{wg}$ for type-0 SPDC. We use these to generate phase matching curves for both signal and idler fields to fit the experimental data shown in Fig. 6(b) and (c). The matching between theory and experiment is remarkably good. An effective length of the entire waveguide of $L_{\text{eff}} = 8.5\,$mm matches the experimental FWHM of type-II SPDC. This length is significantly shorter than the specified nominal length of 15 mm, suggesting possible variation in the waveguide fabrication [20].

The data in Fig. 6(c) is compared to two curves with different grating periods. We can see that a tiny change in the grating period ($\Delta\Lambda = 4\,$nm, $\Delta\Lambda/\Lambda \approx 0.0005$) alters the phase matching wavelengths by a considerable amount ($\Delta\lambda_s \approx 2\,$nm, $\Delta\lambda_i \approx 4\,$nm). We thus believe that the broadening of type-0 SPDC phase matching bandwidth is due to some small non-uniformity in the grating period over the waveguide [20]. As type-II phase matching does *not* depend on periodic poling, a variation in grating period will not affect the bandwidth of type-II SPDC. This is supported by the data matching a single $\text{sinc}^2(\Delta k L_{\text{eff}}/2)$ function in Fig. 6(b). Temperature tuning does affect the type-II SPDC spectra through the temperature dependence inherent in the refractive indices $n(\lambda, T)$ [20], and by altering the waveguide contribution $k_{wg}(T)$, while the temperature dependence of the grating period $\Lambda(T)$ does not affect the type-II spectra because type-II SPDC does not depend on the poling period. In comparison, the type-0 SPDC spectra is affected by the temperature tuning through $n(\lambda, T)$, $k_{wg}(T)$, and also $\Lambda(T)$. We believe the main reason for type-II SPDC to be brighter (both spectrally and overall) than its type-0 counterpart in this waveguide (despite $d_{\text{eff}} > d_{24}$) is that the difficulty in maintaining a uniform grating period and the resulting variations in the grating period along the entire waveguide effectively decreases the phase matching efficiency of type-0 SPDC, with different section of the waveguide producing photon pairs at different wavelengths which do not add up coherently. Since type-II SPDC is immune to the grating period change, it is relatively enhanced compared to its type-0 counterpart.

4. Conclusion

We have demonstrated a potentially useful device for chip-scale quantum information processing by measuring a single PPKTP waveguide's output spectra (single and coincidence) at a range of operating temperatures, pump powers, and phase-matching schemes. The results show a versatile device with a tunable down-conversion bandwidth, together with high spectral brightness and high purity. We have also separated the photon-pair contribution from single-photon fluorescence for both type-0 and type-II SPDC. This single-photon fluorescence may result from defects in the PPKTP crystal such as gray tracking and/or color center formation [6, 44], although a definitive answer is not possible at the moment. A waveguide made from a hydrothermally-grown KTP crystal may produce fewer fluorescence photons than the flux-grown one that we investigated, which can potentially yield a photon-pair source with even higher purity. Improving collection efficiencies (including both free-space and fiber-coupling optics) will boost the collected photon-pair rate, and thus the usable brightness of the source.

The source may also be further spectrally engineered to yield a factorable state. We believe such a versatile source is a promising candidate for future integrated photonic circuitry and chip-scale quantum devices.

Acknowledgement

We thank Dr. Tracy Clement for supplying the Matlab codes for calculating the Schmidt numbers and the values for entropy of entanglement, and Dr. Sergey Polyakov and Dr. Wei Fang for helpful discussions. This work has been supported in part by the Intelligence Advanced Research Projects Activity (IARPA) Polarization-Entangled Photon Source Program, and the Multidisciplinary University Research Initiative Center for Photonic Quantum Information Systems (Army Research Office/IARPA program DAAD19-03-1-0199). A.J.P. acknowledges support from the Intelligence Community Postdoctoral Research Associateship Program.